Geological Society of America
Memoir 195
2002

Three-dimensional anatomy of a geothermal field, Coso, southeast-central California

Jonathan M. Lees
Department of Geology, University of North Carolina, Chapel Hill, North Carolina, 27599, USA

ABSTRACT

This paper reviews geophysical and seismological imaging in the Coso geothermal field, located in southeast-central California. The Coso geothermal production area covers ~6 × 10 km^2. Although regional seismicity is addressed, as it sheds light on the magma, or heat, sources in the field, the primary focus of this paper is on the main production area. Three-dimensional inversions for P- and S-wave velocity variations, distribution of attenuation, and anisotropy are presented side-by-side so that anomalies can be compared spatially in a direct manner. Velocity inversions for P and S waves are combined for direct determination of Poisson's ratio and indirect estimation of variations of porosity in the field. Anomalies southeast of Sugarloaf Mountain are prominent on nearly all analyses. The anomalies coincide with high levels of seismicity and with stress anomalies as determined from earthquake focal mechanism analysis and seismic anisotropy distribution. The anomalies also correlate with high heat flow in the field and the termination of geothermal production to the south. I speculate that an intrusion is present in this region that causes significant perturbation of stress in the field.

THE GEOPHYSICAL IMPORTANCE OF COSO

The importance of Coso, from a geophysical perspective, stems from the fact that it is an evolving geothermal field in its initial stages of economic development rather than in maturity. Furthermore, it is situated on the western edge of the Basin and Range province and along what has been suggested is the newly forming tectonic boundary between the Pacific and North American plates (Nur et al., 1993). As such, the active Coso geothermal field provides a living laboratory for investigating the interaction of fluids, magmatic material, and heat in the Earth.

The installation of a borehole seismic network in the region of the Coso geothermal field in the early 1990s provided a means to collect high-quality microearthquake data while monitoring activity in the field (Fig. 1). Because there is active production of geothermal energy at Coso, there are also high levels of low-magnitude seismic activity recorded daily by the seismic array. The seismic stations at Coso consist of 4 Hz, three-component geophones cemented in boreholes ranging from 30 to 70 m depth, recording at 480 samples/s. By recording away from the surface, signal-to-noise ratios are very high, and events as small as magnitude -1 to -2 are routinely recorded. This provides a high-quality data set that can be used to study structure in the field as well as the dynamics of the evolving field. In this paper, I address structural aspects of the geothermal setting by reviewing and compiling results reported in a series of papers directed at imaging seismological properties in the field (Bhattacharyya et al., 1999; Feng and Lees, 1998; Hough et al., 1999; Lees, 1998; Lees and Wu, 1999, 2000; Wu and Lees, 1996, 1999b).

Arrival times of seismic waves from earthquakes are the simplest and most precise measurements that can be made on seismic records. Location of earthquakes depends on the ability to determine traveltimes of events, which in turn requires knowledge of the seismic velocity structure in the intervening

Lees, J.M., 2002, Three-dimensional anatomy of a geothermal field, Coso, southeast-central California, *in* Glazner, A.F., Walker, J.D., and Bartley, J.M., eds., Geologic Evolution of the Mojave Desert and Southwestern Basin and Range: Boulder, Colorado, Geological Society of America Memoir 195, p. 259–276.

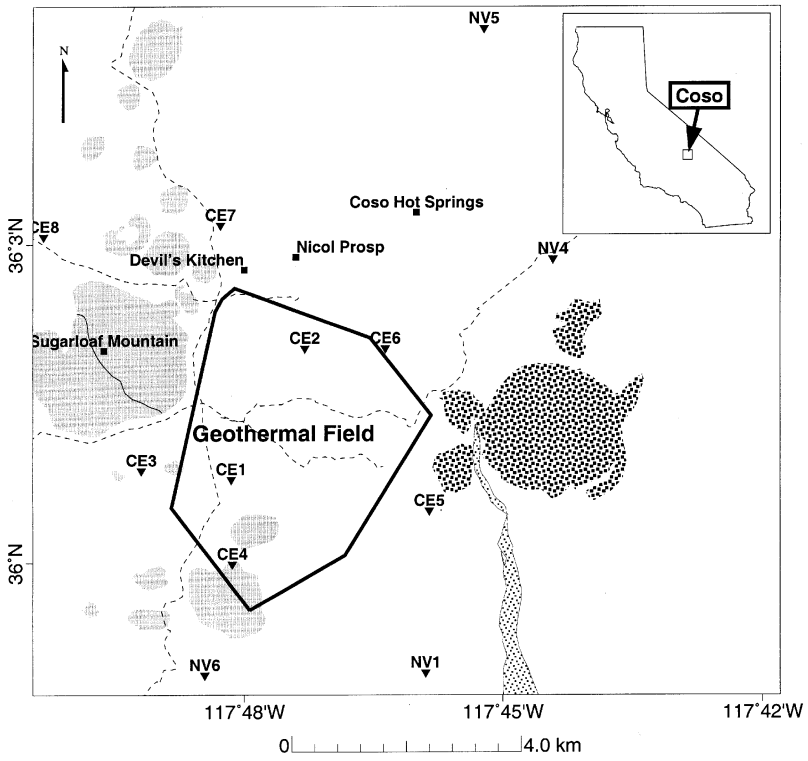

Figure 1. Map view of the geothermal field region at Coso, California. Inset shows location of Coso in California. Circular red features are Quaternary rhyolitic domes. Purple regions are thick, Tertiary andesitic flows, and the green-filled zone is a Quaternary basalt flow. Lines show roads in the geothermal field, outlined by a bold line. Triangle symbols are seismic stations renamed from Table 1 of Wu and Lees (1999b). Important geographic locations are annotated: DK—Devil's Kitchen; NP—Nicol Prospects; CHS—Coso Hot Spring; SM—Sugarloaf Mountain.

media. Generally, earthquakes are located with one-dimensional layered models. It is well known, however, that the Coso geothermal field is three-dimensional. To improve understanding of structural details in the field, a model is sought that explains the data better than the one-dimensional view and that provides information on the three-dimensional variation of seismic properties in the Earth.

Detailed discussions of the methodology used in the studies presented in this paper can be found in a series of papers that outline the tomographic techniques (Lees, 1992; Lees and Crosson, 1989; Lees and Shalev, 1992). Earthquakes are located initially with a one-dimensional layered model, derived by using the method of joint inversion for location and model parameters along with geologic constraints and external data, such as reflection data recorded in the region (E. Shalev, personal communication). In addition to the one-dimensional models, a station correction (constant time shift for each station) is incorporated in the analysis to account for near-station structure or varying station elevations (Wu and Lees, 1999b). To some extent, use of a station corrections helps compensate for inaccuracy of the one-dimensional approximation of the real Earth. Earthquake locations determined with the one-dimensional models show considerable heterogeneity, with significant clustering in those parts of the field where seismicity levels are elevated (Walter and Weaver, 1980; Feng and Lees, 1998).

Once the one-dimensional models and initial locations are established, three-dimensional analyses can be accomplished. It is now common practice to refer to three-dimensional seismic inversion analysis for the determination of varying physical properties as "tomography." This approach is borrowed from the medical sciences, and the methods of CAT (computerized axial tomography) scanning have been adapted to seismic analysis. In actuality, there are significant differences between seismic tomography and medical imaging. In seismology, the relationship between the traveltime and the velocity of the medium can be written simply as

$$\Delta T = \int_r [1/V(s)]\, ds, \tag{1}$$

where ΔT is the traveltime, V is the velocity as a function of the position s along the raypath, and the path integral is taken along the raypath, indicated by "r." The "inversion" is an attempt to extract the velocity given the traveltime data. In equation 1, I have explicitly included the dependence of the velocity on the raypath to emphasize that seismic traveltime tomography is inherently nonlinear because the paths of the rays from the earthquake source to the receivers depend on the model parameters that are being sought. Traditional medical CAT scanning, furthermore, is accomplished by inverting slices of the target region and building three-dimensional models by stacking series of two-dimensional models (the word *tomography* means "slice picture"). In seismology, three-dimensional structures are typically determined via full three-dimensional inversion, and

later they are sliced for visualization purposes. At Coso, ongoing seismic studies include tomographic analysis of attenuation, velocity, and anisotropy. In each of these studies, different aspects of the data are considered and must be treated according to different assumptions. These are outlined here before discussion of specific results for each inversion. The tomography results summarized in this paper were derived from data recorded by the Navy Geothermal Program and Duke University (Peter Malin) from mid-1993 to early 1995. The network includes 16 borehole stations located in the vicinity of the geothermal field (Fig. 1). Depths to the sensors in the borehole stations are typically less than 70 m.

Ultimately, one goal for seismologists is to delineate all relevant three-dimensional seismic properties of this geothermal region. Although global seismologists have been moderately successful at simulating synthetic seismograms at low frequency, the equivalent effort for high frequency at small scales is still practically impossible. This fact is, in part, due to lack of knowledge of three-dimensional variations of properties at the necessary small scales. Tools are currently being developed for examining wave propagation in complex media at high frequency (Wu and Lees, 1992a, 1992b, 1997). High-quality data sets like those available for the Coso geothermal field will prove to be invaluable for future theoretical investigations of seismic waveform propagation.

LOCAL AND REGIONAL SEISMICITY

The Coso area is one of the most active seismic regions of southern California, clearly shown in a density plot of earthquakes in the area (Fig. 2; Walter and Weaver, 1980). According to 1980–1994 earthquake catalogues from the California Institute of Technology (Caltech), recorded earthquake counts in the Coso area are comparable to the most active regions of southern California, including along the San Andreas fault. Seismicity in the Coso geothermal field area has been described in detail by Walter and Weaver (1980), Roquemore and Simila (1994), Alvarez (1992), and Feng and Lees (1998) and from a more regional perspective by Bhattacharyya and Lees (this volume). Several larger events in the region highlight the importance of monitoring seismicity at Coso: the $M_b = 4.0$ event in Rose Valley (Alvarez, 1992), the Ridgecrest events (Hauksson et al., 1995), and more recently the two Coso events (1996 local magnitude $M_L = 5.3$ and 1998 $M_L = 2$) located immediately outside the geothermal field proper (Bhattacharyya et al., 1999). These events are most likely a response to local tectonic stresses associated with Basin and Range extension and North American–Pacific plate margins. For the Coso geothermal field, the most notable observation is the relatively shallow (less than 5–6 km) seismicity below the field itself. Deep earthquakes (down to 12 km depth) surround the Coso geothermal field, primarily in the form of clusters associated with larger ($M_L > 4$) events.

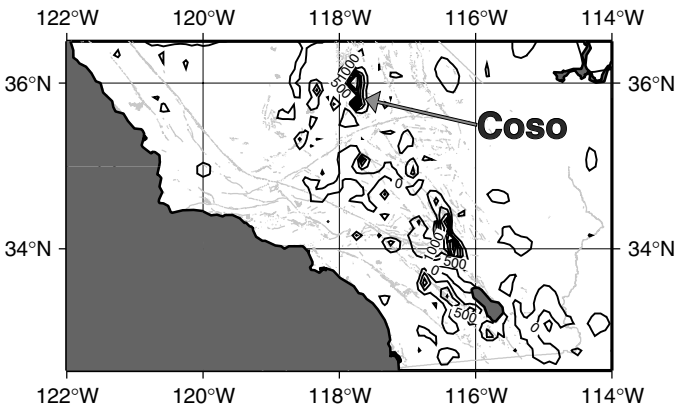

Figure 2. Density contours of 1980–1994 southern California earthquakes with magnitudes greater than zero. Catalogues were extracted from the California Institute of Technology database. The Coso–Ridgecrest area is one of the most actively seismic regions in southern California.

By using ~40 000 events from the Caltech–U.S. Geological Survey (USGS) seismic network in southern California (1988–1998), I have mapped the depth extent of seismicity in the vicinity of Coso. (Hypocenters located from the borehole array at Coso were not used here because they are nearly all shallow. By using only events from one data source, catalogue uniformity is preserved.) Contours of seismicity cutoffs (i.e., the maximum depth of seismicity) span a region 10–12 km east-west and 8 km north-south, bounded to the west by the geothermal field and extending eastward several kilometers (see contours in Fig. 3). The fact that the seismicity contours in the vicinity of the field become shallower is presumably associated with reduction in brittle behavior of the rocks due to the emplacement of magma and/or elevated heat flow (Walter and Weaver, 1980).

A region of particularly intense activity is seen in the southwestern part of the field, close to the south side of Sugarloaf Mountain. As is shown subsequently, this zone coincides with the location of anomalous attenuation, velocity, and anisotropy in the field. Although the regional shallowing of seismicity may represent a large anomaly that has heated over time, the concentrated seismicity in the southwest part of the field may represent a shallow intrusion affecting the brittle crust. The high heat flow observed in this corner of the field (Combs, 1980) further suggests that this is the locus of a concentrated anomaly.

It is interesting that Feng and Lees (1998) noted that the distribution of seismicity within the geothermal field showed no considerable change in seismicity rates associated with the 1992 Landers event, in contradiction to the finding of Roquemore and Simila (1994). The discrepancy lies in how the events are selected. Feng and Lees considered the geothermal field to be the area enclosed with the bold line in Figure 1, thus excluding the Ridgecrest events and their aftershocks. Expansion of the region southward would include areas that were affected after the Landers rupture.

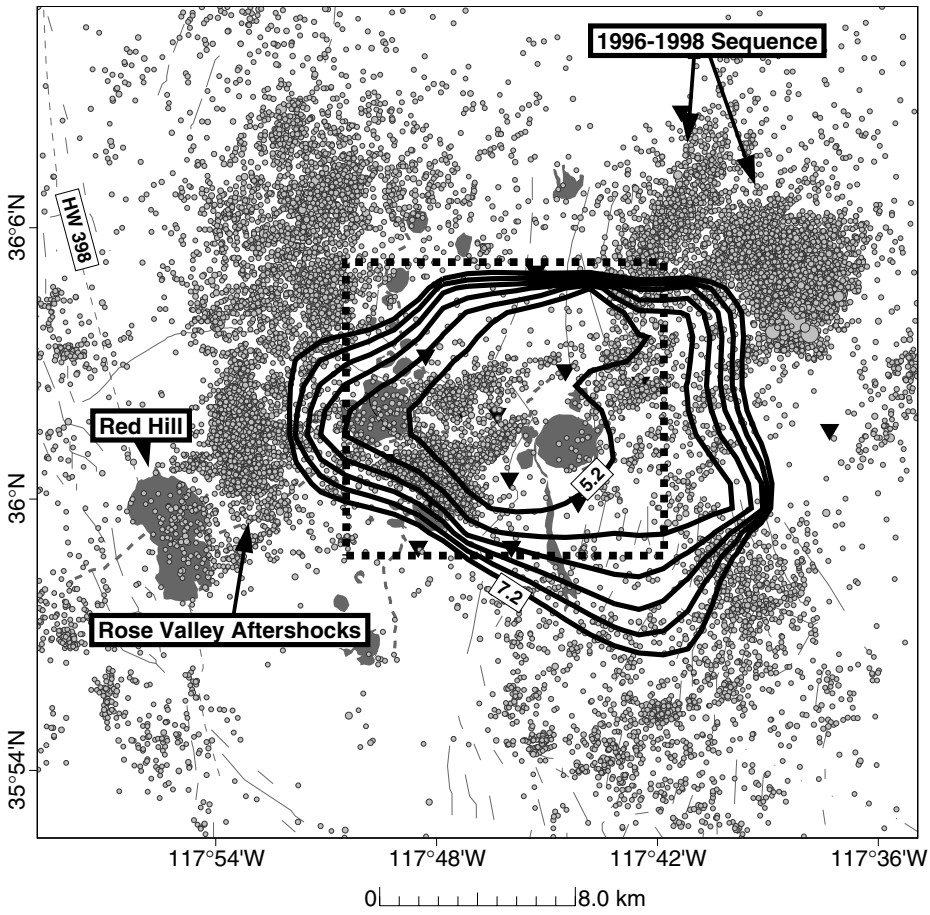

Figure 3. Map of regional seismicity from the Caltech-USGS southern California seismic array. Contours show the maximum depth of seismicity in the Coso area based on regional seismicity. Contour interval is 400 m; the labels 5.2 and 7.2 refer to depth in kilometers. The geothermal area and region of the tomographic analyses (Fig. 1) are outlined by dashed line. Geographic features are the same as in Figure 1 with the addition of Red Hill, a volcanic cone located along Highway (HW) 398. A large cluster of shallow events is located southeast of Sugarloaf Mountain (large rhyolite dome) where numerous anomalies are observed on the tomographic analyses. Clusters outside of the geothermal field include the Rose Valley sequence west of Sugarloaf and the 1996–1998 sequences described in Bhattacharyya et al. (1999).

PREVIOUS GEOPHYSICAL ANALYSIS AT COSO

Three-dimensional analysis of the Coso region began in the late 1970s and early 1980s. Three-dimensional teleseismic inversions (Reasenberg et al., 1980; Walck and Clayton, 1987), gravity modeling, electric field methods (Jackson and O'Donnell, 1980), and seismicity studies (Walter and Weaver, 1980) were used to reconnoiter in a region not heavily studied previously. This initial body of work was later expanded on by efforts to characterize Vp/Vs ratios in the Coso–Indian Wells Valley region (Walck, 1988) and attenuation structure of the same region (Ho-Liu et al., 1988; Sanders et al., 1988). The main goal of these studies was to delineate the heat sources of the field: what was expected was a lowering of velocity in regions where rocks are particularly hot, especially where a large fraction of melt may be present. Another expectation was a considerable reduction of shear-wave amplitude where significant percentages of melt exist. Although these studies suggest that the heat source at Coso is fairly shallow, and there appears to be a signal-reducing velocity in conjunction with wave-amplitude attenuation, the results had relatively crude resolution (tens of kilometers), and the quality of the data was poor compared to the borehole data discussed in this paper. Subsequent high-resolution studies in the geothermal field itself, discussed in detail in the next section, reveal complex structures associated with geothermal fluid flow and intrusion of magma.

HIGH-RESOLUTION SEISMIC VELOCITY INVERSION

Tomographic analysis for velocity anomalies begins by locating earthquakes (sources), usually with one-dimensional models. Raypaths from sources to receivers are calculated, and the target region is divided, or parameterized, into small cells. For each raypath, a weighting function is determined that estimates the influence the data for that ray have on the cells in the model that the ray traverses. For block models, this procedure amounts to estimating the penetration length of each cell the ray intersects. The traveltime residuals, i.e., the difference between the predicted traveltime and the observed traveltime, are then projected along the raypath along the cells according to the weighting function. In the computer, this process can be expressed as a large, sparse matrix inversion. Because the raypaths and the earthquake locations depend on the velocity models, the inversion is nonlinear, and the solution is achieved by iteration of linearized inversions that converge to the final so-

lution. The size of the matrices can often be quite large (50 000 model parameters), and model resolution and error bars are usually estimated via computational approximations and simulations.

In the Coso geothermal region, high-precision P- and S-wave traveltimes from 2104 microearthquakes with focal depths of <6 km were used in a nonlinear inversion to derive high-resolution three-dimensional compressional- and shear-velocity structures (Wu and Lees, 1999b) (Figs. 4 and 5). The block size used in the inversions was 0.2 km horizontally and 0.5 km vertically. The microearthquake data allowed for imaging of the top 4–5 km. Spatial resolution was estimated in well-resolved regions to be 0.35 km for Vp and 0.5 km for Vs analyses. Model uncertainties were determined by using the "jackknife" approach, a method involving statistical subsampling of the data to assess the influence that noisy data has on the results (Lees and Crosson, 1989). Average errors in Vp and Vs perturbations were 0.4% and 0.8%, respectively.

The full inversion results are presented as horizontal and vertical cross sections through the three-dimensional models. Low-velocity zones for both P and S waves were identified at geothermal-production depths (1–3 km). A large low Vp (-6%) zone was found 2–2.5 km beneath the triangular region bounded by stations CE1-CE3-CE4 where high attenuation was also found. A high Vp zone was seen under Coso Hot Spring with a slightly contrasting low Vs zone (Figs. 6 and 7), characteristic of fluid saturation. In general, the overall distribution of Vp and Vs perturbations do not correlate directly. An isolated high Vs ($+9\%$) feature, $\sim$2 km in diameter, was delineated between stations CE2 and CE6, extending from the surface to the deeper parts of the model. This feature is surrounded by a circular, low-Vs belt with a width of $\sim$1 km. This belt was interpreted as a cracked, high-porosity reservoir and/or conduit for geothermal fluid. In the CE1-CE3-CE4 region, contrary to low Vp, a broad high-Vs zone was observed at geothermal-production depths, from 1 to 2.5 km.

POISSON'S RATIO AND POROSITY

Perturbations of velocity is one way to view the three-dimensional variation of properties in the target region, but it is often useful to consider alternative combinations of the acoustic parameters that may be sensitive to different physical properties. As a follow-on to the description of Coso velocity perturbations and their respective relationship to lithologic and hydrothermal distributions in the field, perturbations of the Vp/Vs ratio and the $\Pi = \text{Vp} \times \text{Vs}$ product can be used to determine Poisson's ratio and porosity (Lees and Wu, 2000). Poisson's ratio is the ratio of the fractional lateral contraction to the fractional longitudinal extension and depends on lithology and fluid saturation. Poisson's ratio σ is related to $r = \text{Vp/Vs}$ by

$$\sigma = (r^2 - 2)/[2(r^2 - 1)], \tag{2}$$

and thus r is a proxy for Poisson's ratio. Porosity, on the other hand, is more difficult to estimate because there is no a simple analytical relationship between porosity and velocity. Lees and Wu (2000) used studies of the relationship of porosity and Π in sedimentary rocks (Pickett, 1963; Tatham, 1982) to estimate the distribution of porosity at Coso. Although for sedimentary rocks, porosity is introduced by pore spaces inherent in the fabric, at Coso, on the other hand, cracks and fractures are assumed to be analogous to the pore structures of the sediment, thus providing an analogous mechanism for spatial variations of Π to be related to porosity changes. The velocity combinations thus help delineate zones of intense heat, fracture accumulation, and fluid saturation. I summarize the results in Figures 8, 9, 10, and 11, although detailed descriptions of Vp/Vs and Π inversions and interpretations can be found in Lees and Wu (2000).

The average Poisson's ratio at Coso was estimated to be 0.224, lower than the crustal average of 0.25. Two major features with low Poisson's ratio and low porosity were identified at geothermal-production depths (1–3 km) near stations CE2-CE6 and CE1-CE3-CE4 (Figs. 8 and 9). These two low-σ, lower-porosity features are separated by a northwest-trending, arcuate band having a high Poisson's ratio and high porosity. The diameter of this circular structure is 0.8–1.2 km. Because of the correlation to the low-Π anomalies (Figs. 10 and 11), it is interpreted as a potentially highly porous feature suspected to be fluid saturated (obviously correlated to the Vs tomography results in Figs. 5 and 6). My interpretation of this feature is that it most likely represents a conduit or reservoir of geothermal fluids. The east-west and north-south arms of the arc correlate well with observed mainstream fluid-flow directions and are probably primary avenues through which hot water is transported from the heat center around stations CE1-CE3-CE4 (Lees and Wu, 2000; Leslie, 1991). The vertical, low-σ and high-Π channel beneath the triangular region defined by CE1-CE3-CE4 corresponds to a high-attenuation feature found in the attenuation inversion described next. On the basis of the tomographic analyses, I interpret this feature as the hot, unfractured core of the last major magmatic intrusion in the Coso geothermal field.

P-WAVE ATTENUATION

Although simple traveltimes provide the basis for velocity analysis, the amplitudes and the frequency content of seismic waves contain rich information on the absorption of seismic energy in the intervening media. Seismic velocity tends to be a relatively insensitive estimator of temperature variations in rocks. Attenuation, on the other hand, is a relatively sensitive indicator of rock temperature. Usually physicists measure the "quality factor" of materials, i.e., the efficiency of the material to pass energy at a particular frequency. The quality factor, Q, is defined as the ratio of stored to dissipated energy in material as seismic waves propagate through. Attenuation is then defined

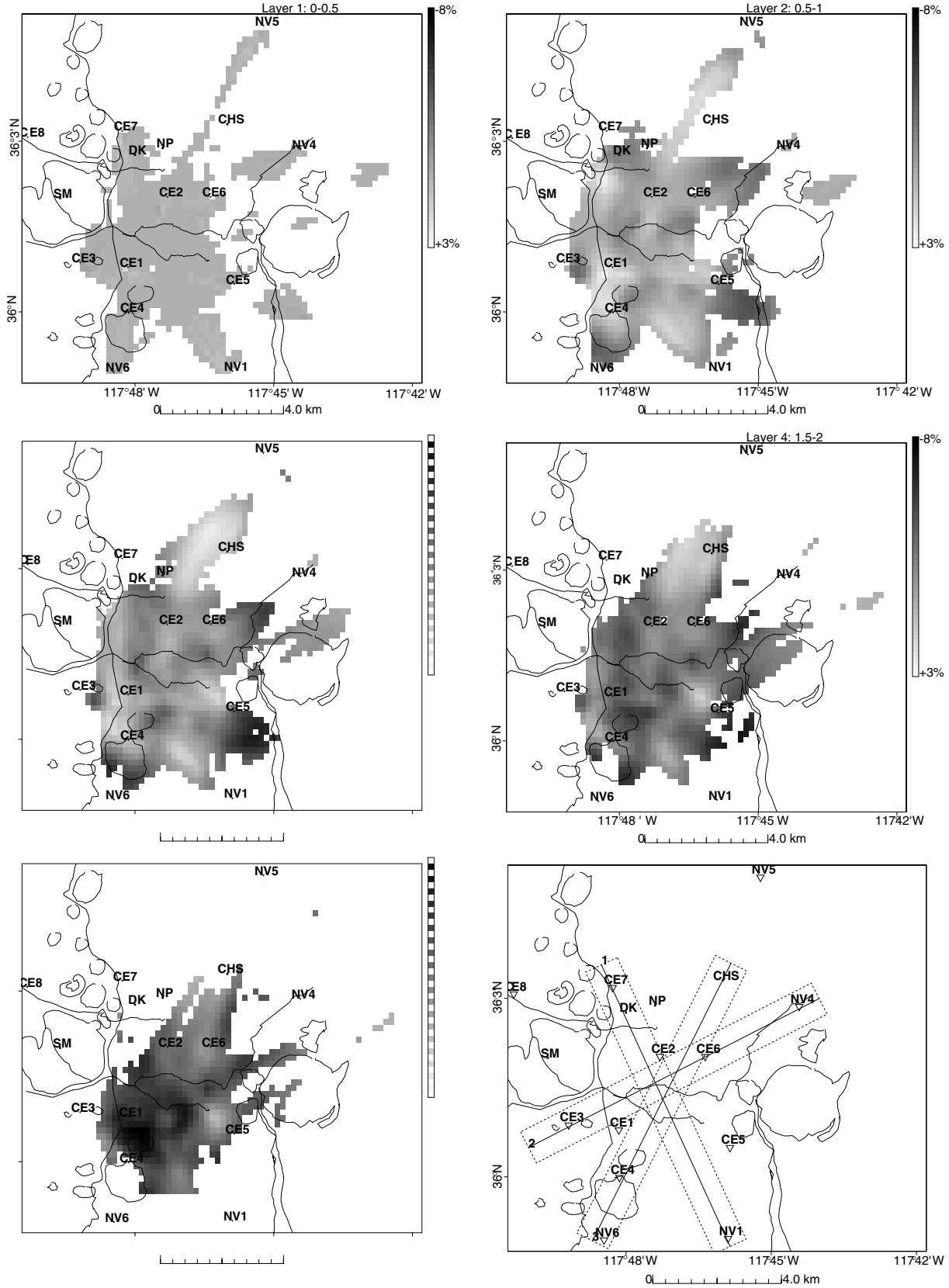

Figure 4. Tomographic analysis of P-wave anomalies in the Coso geothermal field. Light areas show positive velocity perturbations representing higher-velocity zones. Dark areas have relatively lower velocity. Blocks that are not sampled are blanked out (white). Map features and stations are plotted for geographic reference (see Fig. 1). Map orientations of cross sections 1, 2, and 3 (numbered) are presented in lower right map for reference in subsequent cross-section figures. Layers are numbered, and the depth in kilometers that they represent is shown at the top of each map.

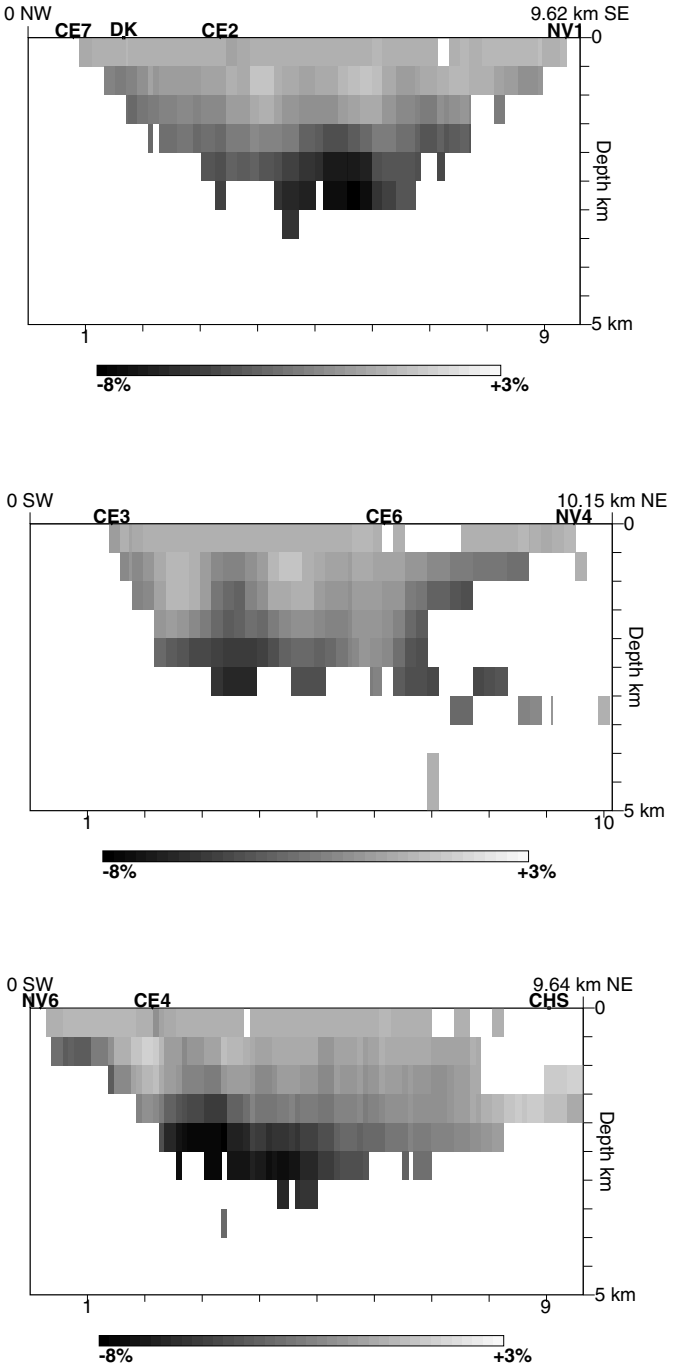

Figure 5. Vertical cross sections of P-wave anomalies in the Coso geothermal field. Locations of cross sections are presented in Figure 4, lower right.

as the reciprocal of Q and thus represents a measure of the absorption or loss of energy in the seismic waves as they pass through intervening material. Q values range typically from 10 to 100 in laboratory measurements on sandstones and 100–1000 in igneous and metamorphic rock measurements (Johnston et al., 1979). These measurements, naturally, are performed on simple samples and do not take into account large-scale structures, fractures, and mixtures.

Attenuation usually comes in two guises: intrinsic and scattering. Intrinsic attenuation relates to losses associated with heat and friction. Scattering attenuation is due to losses from waves diffracted throughout the medium as they propagate from source to receiver. For the Coso geothermal field, it was shown that intrinsic absorption, as opposed to scattering, appears to be the dominant attenuation factor, at least in the upper 4 km (Wu and Lees, 1996). This result implies that three-dimensional Q variations may be interpreted as being related to intrinsic physical properties of the rocks such as lithology, temperature, and porosity.

In a study of Q distribution at Coso, Wu and Lees (1996) used P-wave pulse widths to estimate the three-dimensional distribution of attenuation in the geothermal field (Figs. 12 and 13) They used pulse width broadening to estimate loss of energy in seismic P-wave arrivals that can be shown to be linearly related to Q^{-1} if microseismic sources are assumed to be impulsive or nearly so (Wu and Lees, 1996). The equations for deriving (inverting for) a three-dimensional quality-factor distribution are nearly identical to the formulas used to derive three-dimensional velocity in equation 1. Once the velocity is determined, three-dimensional raypaths are calculated in the three-dimensional model, and the quality factor is linearly related to the attenuation of seismic waves along each path.

The average Q in the Coso geothermal area was estimated to be ~49. A broad region of low Q (30–37) was identified at 0.5–1.2 km depth below Devil's Kitchen, Nicol Prospects, and Coso Hot Springs. Another larger and deeper (2.5–3.6 km) low-Q feature was observed 2–3 km southeast of Devil's Kitchen and Nicol Prospects. This feature was interpreted as the main origin of Coso's hydrothermal energy and may be related to a suspected rising magma accumulation although the vertical extent of the presumed magma body is not defined by the current data set. Southwest of Devil's Kitchen and Nicol Prospects, a vertical, low-Q channel ~1 km in width and connecting the deeper to the shallower regions of low Q was identified and may be a conduit supplying geothermal energy to the surface at Coso Hot Springs.

An independent study of Q can be accomplished by examining the distortion of the frequency spectrum of the P or S wave trains. In this approach, the source spectrum has specific characteristics that must be either assumed or derived, and deviations in the observed spectrum are attributed to attenuation of the waves during transmission (Hough, 1997; Lees and Lindley, 1994). At Coso it has been observed that numerous earthquakes are very similar in waveform, forming clusters of events called multiplets (Lees, 1998). The high-resolution locations from these multiplet earthquake clusters were used to estimate Q via frequency-spectrum methods. The results agreed with pulse-broadening results already described that put a low-Q anomaly ~1 km in the region of high heat flow in Coso (Hough

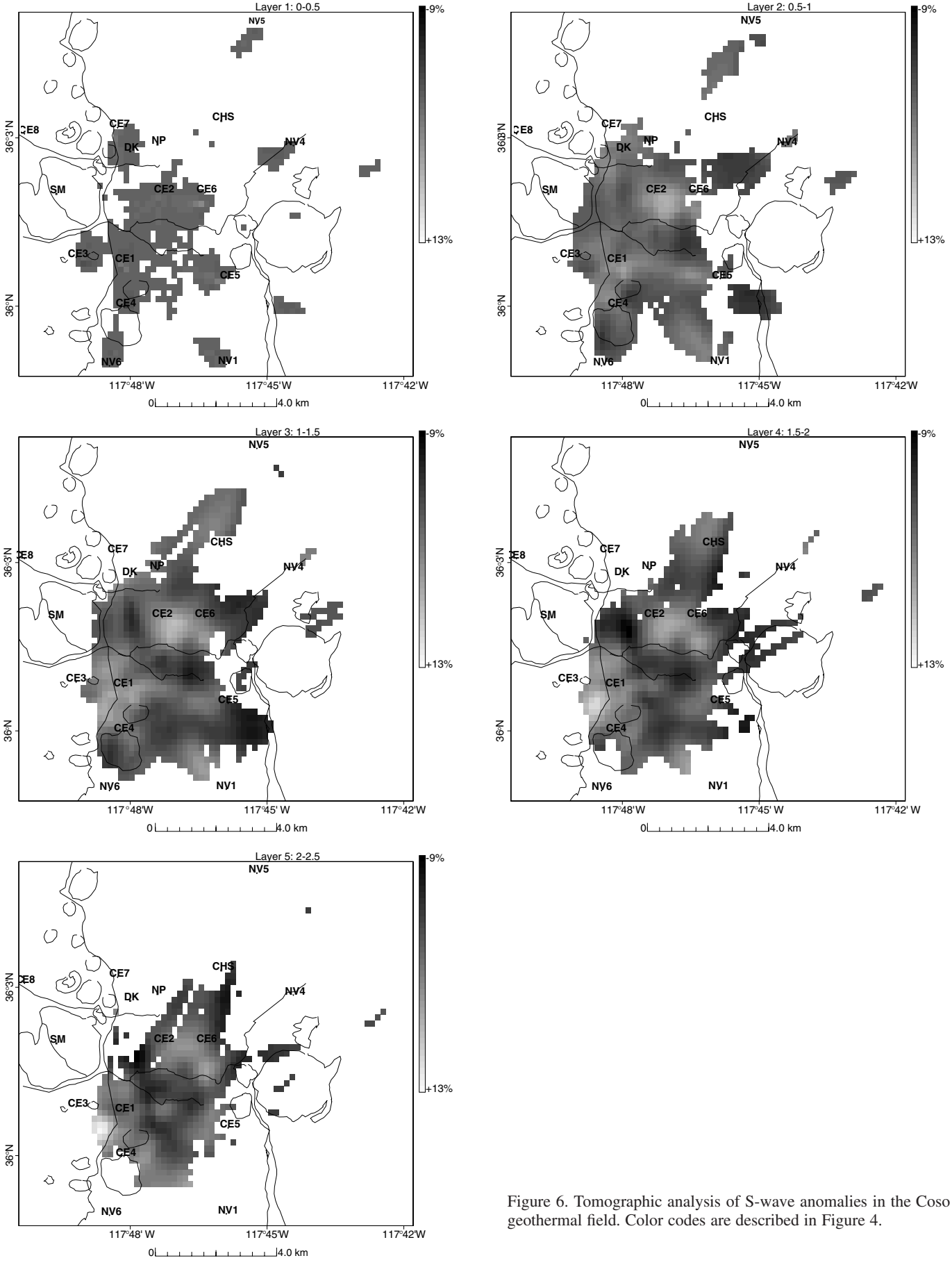

Figure 6. Tomographic analysis of S-wave anomalies in the Coso geothermal field. Color codes are described in Figure 4.

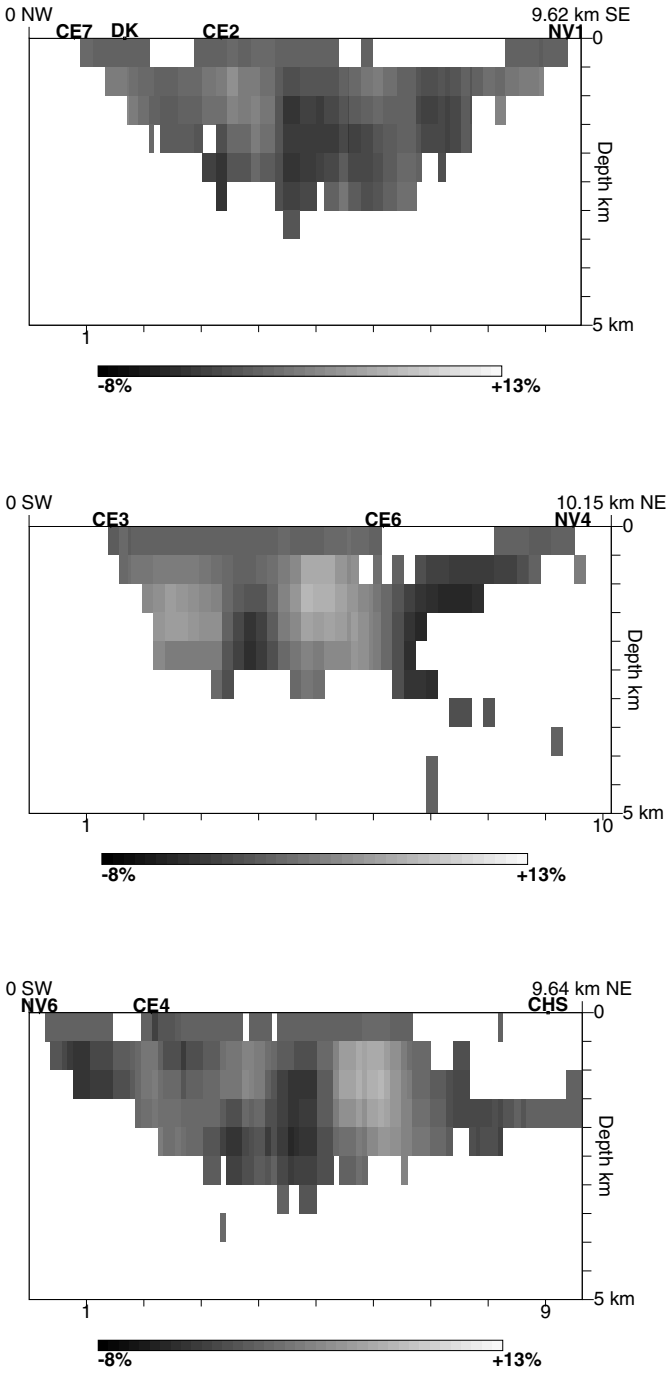

Figure 7. Vertical cross sections of S-wave anomalies in the Coso geothermal field. Locations of cross sections are presented in Figure 4, lower right.

et al., 1999). Unfortunately, very few data were available for this analysis, and thus resolution was poor.

P-WAVE ANISTROPY

Since 1980, seismic anisotropy has been studied extensively in the Earth's crust and upper mantle. The effects of anisotropy on seismic waves are complex compared with the isotropic inhomogeneities (Anderson, 1989; Babuska and Cara, 1991) and therefore should be studied in any investigation of three-dimensional variations of seismic parameters. In geothermal fields, velocity anisotropy was previously observed and associated with fracture zones (Leary and Henyey, 1985; Lou and Rial, 1997). Both internal rock fabric and external physical conditions give rise to velocity anisotropy. Possible origins include preferred crystal orientation, lithologic layering, crack alignment, deviatoric stress field, and fluid flow (Schön, 1996). For the Coso region, I suspect that all these effects influence observed anisotropy to some extent. The preponderance of significant fractures in the geothermal field suggests that fractures, cracks, and ambient stresses are the dominant factors at Coso. A material containing an aligned system of cracks is effectively anisotropic for elastic waves, whereas materials containing randomly oriented microcracks exhibit bulk isotropy (Crampin, 1984; Hudson, 1981, 1994). Application of a deviatoric stress can preferentially open and close cracks, however, depending on their orientation with respect to the principal stress directions (Nur, 1971). The resultant nonuniform crack orientation distribution can introduce elastic anisotropy into an otherwise isotropic material (Nur and Simmons, 1969). Measurements of velocity anisotropy have been used to derive the density distribution of crack orientation, which can be used in turn to predict permeability anisotropy for fluid flow (Gibson and Toksoz, 1990). Researchers modeling geothermal-field evolution would like to have access to this information that will ultimately provide constraints on forward modeling of fluid flow in the crust.

Most researchers have concentrated on anisotropy associated with shear waves traveling through media. These waves are differentially polarized after passing through the anisotropic region, and information relating the level and direction of anisotropy can be determined from analysis of two separated shear waves. This kind of analysis was applied at Coso by Lou and Rial (1997), and three-dimensional variations of shear-wave splitting were determined and used to estimate crack density. The data available for such a study, though, are limited for tomographic analysis because the data must lie within a specific cone beneath the station in order to record the shear-wave splitting, thus limiting the three-dimensional resolution of the analysis. Tomographic inversions generally require large data sets with extensive crossing ray paths to achieve good reduction of noise and proper reconstruction of anomalous bodies. To this end, a new method was developed for investigating three-dimensional variations of P-wave anisotropy (Lees and Wu, 1999; Wu and Lees, 1999a). The much larger data set of P-wave arrivals versus S-wave arrivals at Coso make this an attractive alternative to the shear-wave splitting approach.

Solving for P-wave anisotropy involves solving for six parameters in each sampled block of the target model. The anisotropy is represented as a velocity ellipsoid, or a 3×3 symmetric matrix. The anisotropy ellipsoid is thus fully described by three velocity vectors in the fast, intermediate, and slow

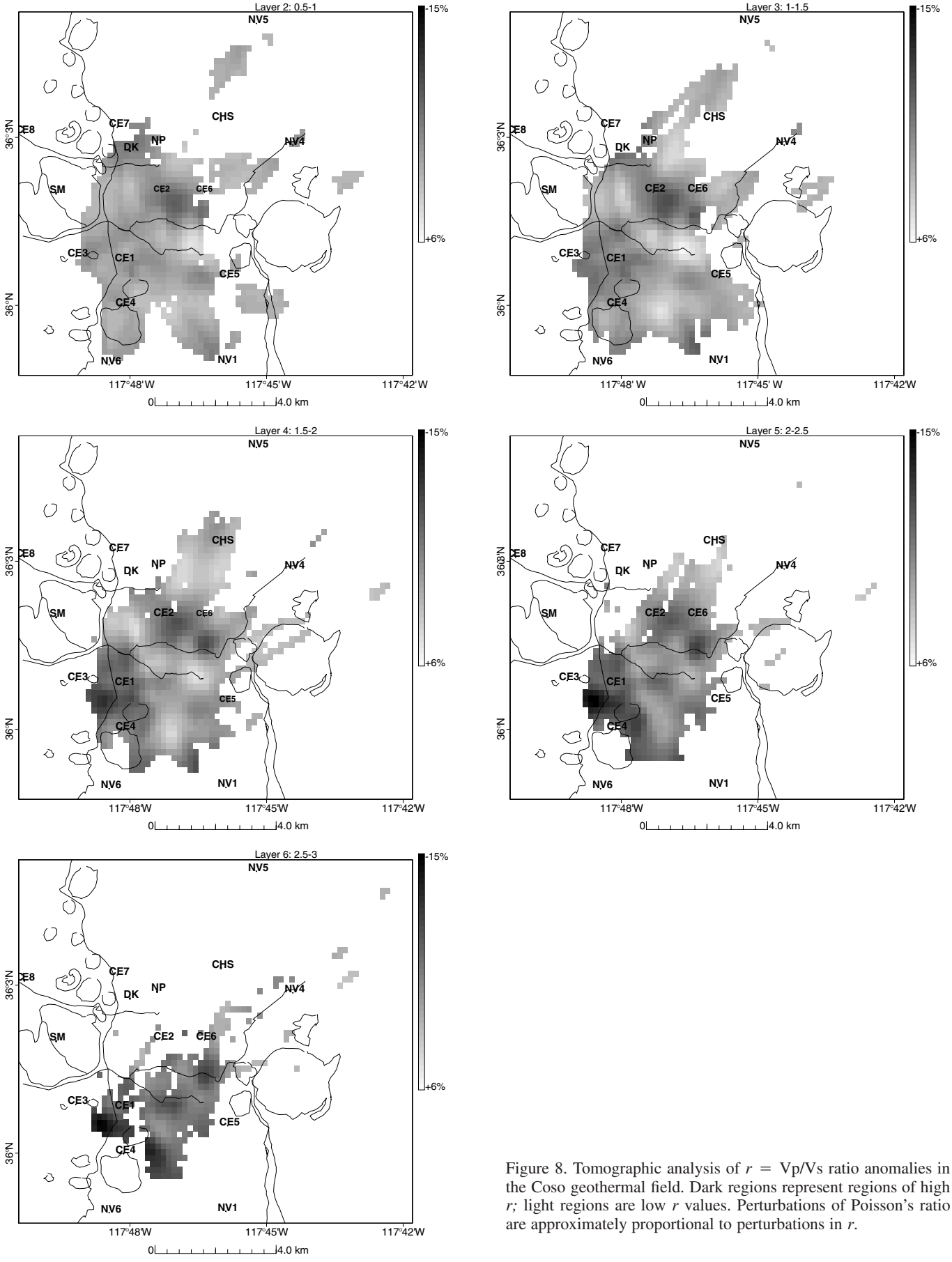

Figure 8. Tomographic analysis of r = Vp/Vs ratio anomalies in the Coso geothermal field. Dark regions represent regions of high r; light regions are low r values. Perturbations of Poisson's ratio are approximately proportional to perturbations in r.

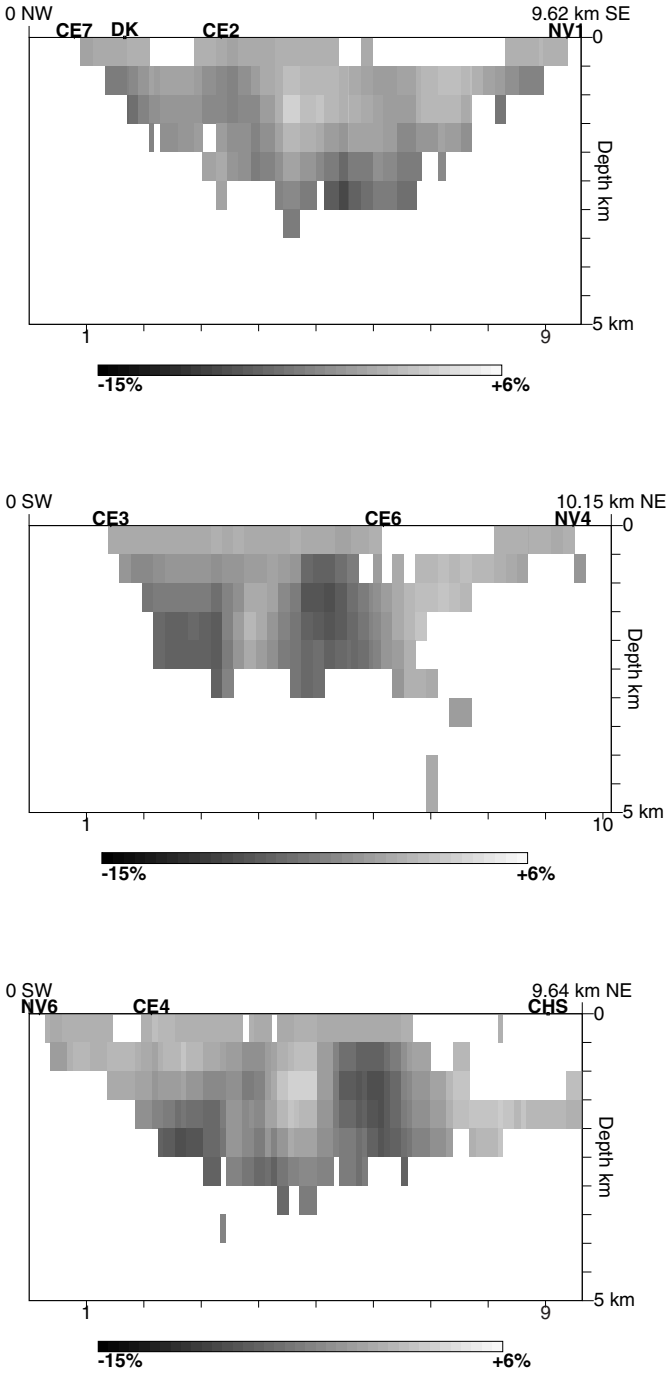

Figure 9. Vertical cross sections of r = Vp/Vs ratio anomalies in the Coso geothermal field. Locations of cross sections are presented in Figure 4, lower right.

directions. To simplify the visualization and interpretation of this set of parameters, the quantity a_f, or the "anisotropy factor," is introduced as the difference between fast and slow velocities divided by the average velocities in a block. The velocities are the eigenvalues of the anisotropy matrices for each block. I present here the three-dimensional distribution of a_f in the Coso geothermal field. Maps of the directions can be found in Lees and Wu (1999).

The overall anisotropy at the Coso geothermal field is north-south fast in the western part and east-west fast in the eastern part (Lees and Wu, 1999). A large-amplitude (8%) anisotropy anomaly was observed at depth east of stations CE1-CE4 (Figs. 14 and 15). An irregular, east-trending anisotropic transition band of 1–2 km width is identified at depth between CE5 and CE6. A dome-shaped structure is found below the triangular area bounded by CE1-CE3-CE4. The stress distribution and crack densities were estimated from the P-wave anisotropy results. Gross features of the anisotropy distributions (e.g., a significant anomaly located below the southwestern part of the field) correlate well with variations of stress inferred from earthquake focal mechanism studies. Feng and Lees (1998) found that the southwest cluster had an anomalously low vertical stress component, as compared to clusters of events north and east. Furthermore, deviatoric stress distribution was found to correlate closely with the high seismicity observed in the southwest part of the geothermal field.

I cannot say for sure, at this time, what the source of the anisotropy is at Coso. I expect that, in a geothermal setting, crack distribution rather than deviatoric stress will be the major contributor to anisotropy variations. For example, if it is assumed that 20% of the velocity anisotropy is attributable to the contemporary stress field, a total differential stress distribution of ~3 MPa is found for the geothermal field on average and nearly twice as much (~6 MPa) in the CE1-CE3-CE4 region. The largest concentration of stress was seen at the suspected intrusion or upwelling center CE1-CE3-CE4, consistent with a proposed magmatic intrusion model for this region based on seismic attenuation (Wu and Lees, 1996). Focal mechanisms and their spatial distribution further support partitioning of stress throughout the geothermal field and emphasize the unusual stress orientation in this part of the field (Feng and Lees, 1998).

Contrary to widely held assumptions, it can be shown that only the residual, unbalanced crack-density distribution produces velocity anisotropy (Wu and Lees, 1999a). Thus, only the deviatoric part of crack density can be determined from the velocity anisotropy, which, in turn, determines the anisotropic part of the permeability orientation. The estimated residual crack densities for the Coso region agree with a previous S-wave splitting study (Lou and Rial, 1997), ranging from 0.0078 to 0.041. By using the median crack density from the P-wave and the S-wave results, Lees and Wu (1999) showed that the average aspect ratio for cracks in the field should be ~1:38. Given an average crack aspect ratio and an estimated crack density, the residual permeability distribution can be estimated by assuming a simple planar fluid-flow model through flat cracks (Gibson and Toksoz, 1990). On the basis of these assumptions, Coso geothermal field permeability can be shown to be roughly proportional to velocity anisotropy (Figs. 14 and 15) (Lees and Wu, 1999). At this point I do not have enough

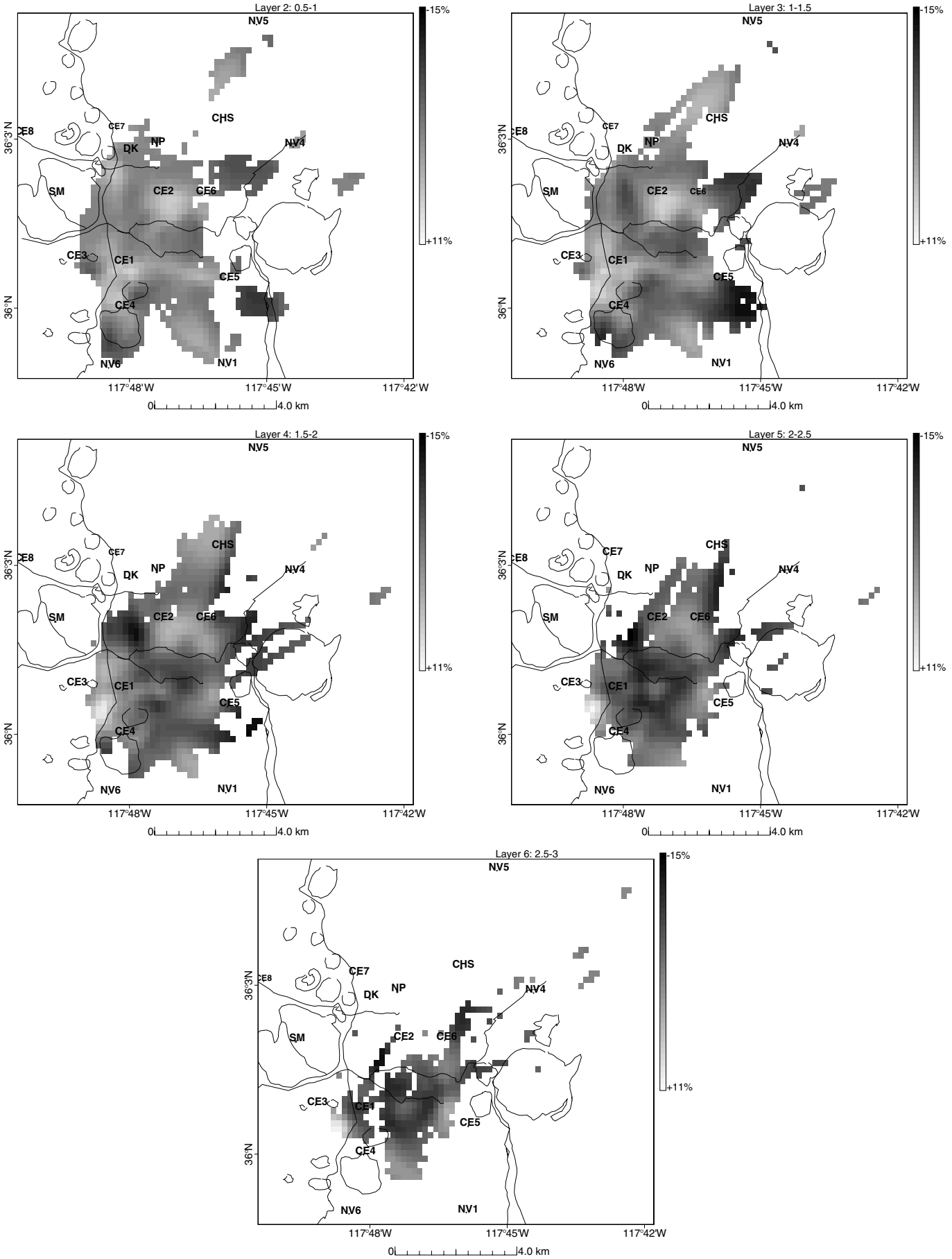

Figure 10. Tomographic analysis of anomalies in $\Pi = Vp \times Vs$ product (a proxy for porosity, Π) in the Coso geothermal field. Dark areas are high Π; light are low Π. High Π is interpreted to indicate low porosity, and low Π is high porosity.

detailed information to verify these predictions. However, they stand as testable hypotheses that can be explored as further studies of the field unfold.

DISCUSSION

The microearthquake data set acquired by the Navy Geothermal Program is one of the most detailed and high-quality data sets for investigating structure in a geothermal setting. Borehole seismic installations, station-density coverage, and high seismicity levels insure a robust database to permit detailed, reliable analysis of structural and dynamical processes in the field as injection and production continue.

There are several significant anomalous features in the Coso region that should be investigated more intensely, e.g., the small triangular area defined by stations CE3-CE4-CE1 deserves greater attention because it correlates well with high heat-flow gradients measured at the surface in the late 1970s (Combs, 1980). Velocity, attenuation, anisotropy, and stress anomalies were each found in the southwestern part of the field and suggest that this area is a focal point for heat flux in the field. I speculate that this narrow zone represents an intrusion of some sort below the active geothermal region. Perhaps it is the peak of an intrusion of magmatic material that extends more broadly at depth to the east, as suggested by the shallow seismicity cutoff that extends in that direction. Furthermore, reflections south of station CE4 suggest that there is a considerable contrast of material properties (elastic impedance) across a subsurface boundary to the south (Lees, 1997). Studies of stress distribution in the field (Feng and Lees, 1998) suggest that there is zonation, or stress partitioning, indicating barriers within the field, perhaps channeling fluid migration.

The overall tomographic inversions for attenuation and anisotropy are not as well correlated as inversions for Vp, Vs, Poisson's ratio, and velocity product, Π. This problem may be partially attributed to the fact that the data quality available for simple velocity analysis is considerably less noisy than the amplitude data used for attenuation studies or the traveltime residuals used to determine P-wave anisotropy. On the other hand, the physical parameters considered may be sampling other aspects of the material traversed and rendering simple geographic correlation fruitless. For example, although attenuation of seismic waves may be very sensitive to temperature, Vp may be more affected by lithologic variations, and anisotropy may be a response to either stress variations or crack density. Anisotropy observed in shear waves may have a different source than that observed for compressional waves. This possibility makes interpretation difficult and open to challenge. My approach here has been to consider several factors and consider external geophysical information where available.

A considerable effort has been invested in imaging details of the Coso geothermal field, including developing new methodology for analyzing three-dimensional variations of seismic properties and their geologic significance. The upper 4–5 km

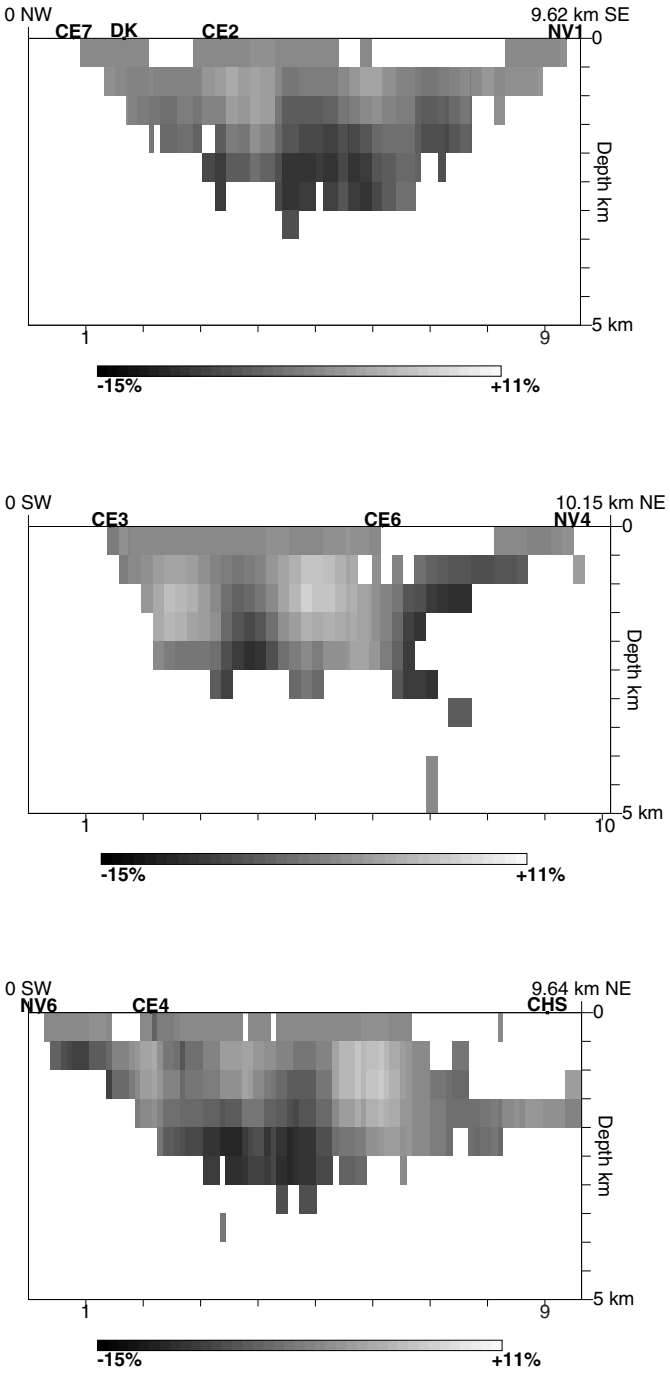

Figure 11. Vertical cross sections of anomalies in Π = Vp $\times$ Vs product in the Coso geothermal field. Locations of cross sections are presented in Figure 4, lower right.

in the field show significant three-dimensional variations in seismic velocity, attenuation, and anisotropy that appear to be related to natural geothermal activity as well as to commercial production in the field. It is clearly evident that significant heat sources and, perhaps, fluid flow in or below the field constitute the ultimate underlying causes of the anomalous features de-

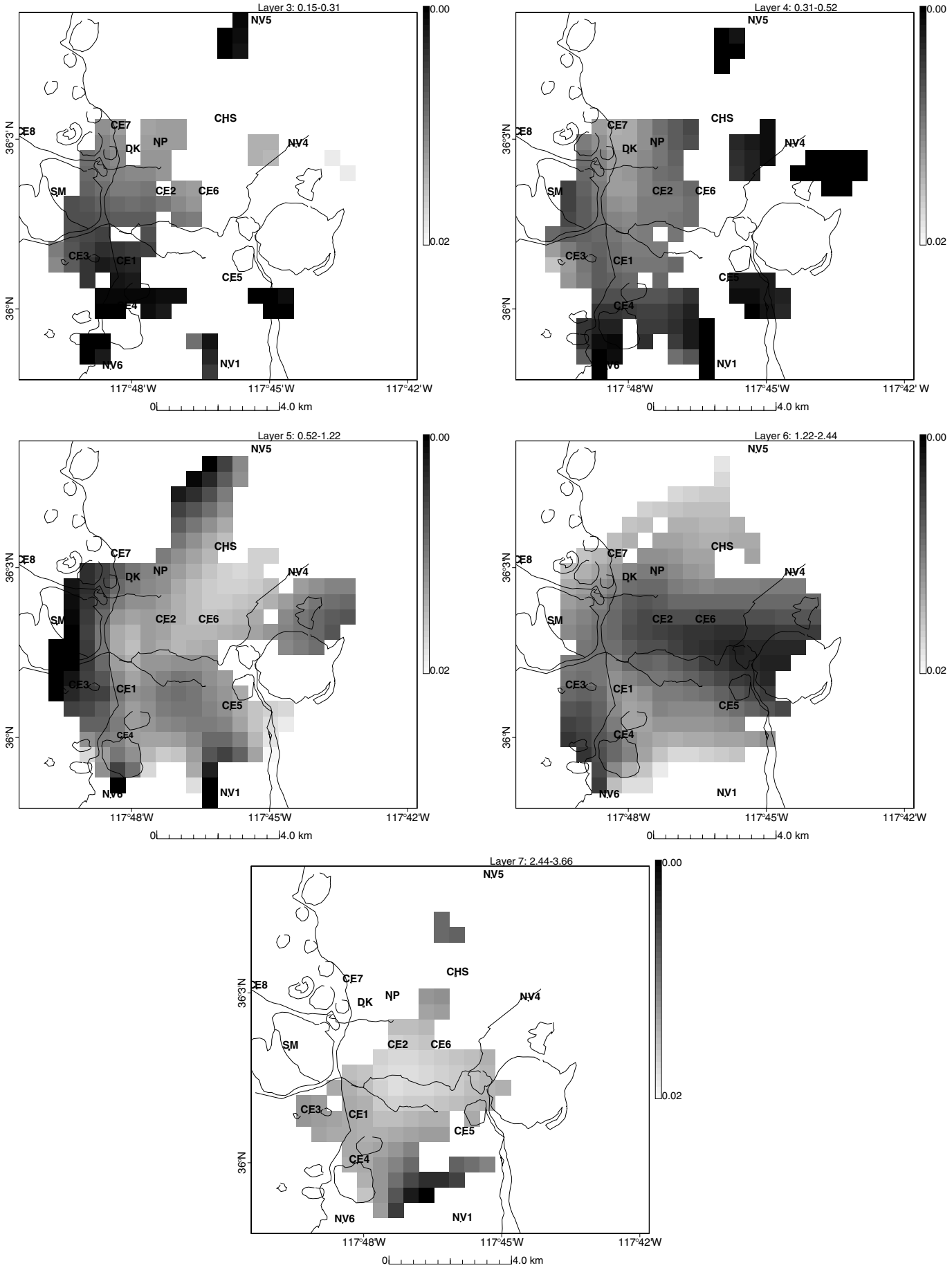

Figure 12. Tomographic analysis of P-wave attenuation anomalies in the Coso geothermal field. Attenuation is the reciprocal of the quality factor Q. Light regions have high Q (small $1/Q$, i.e., lower attenuation), and dark zones have low Q (large $1/Q$, i.e., higher attenuation).

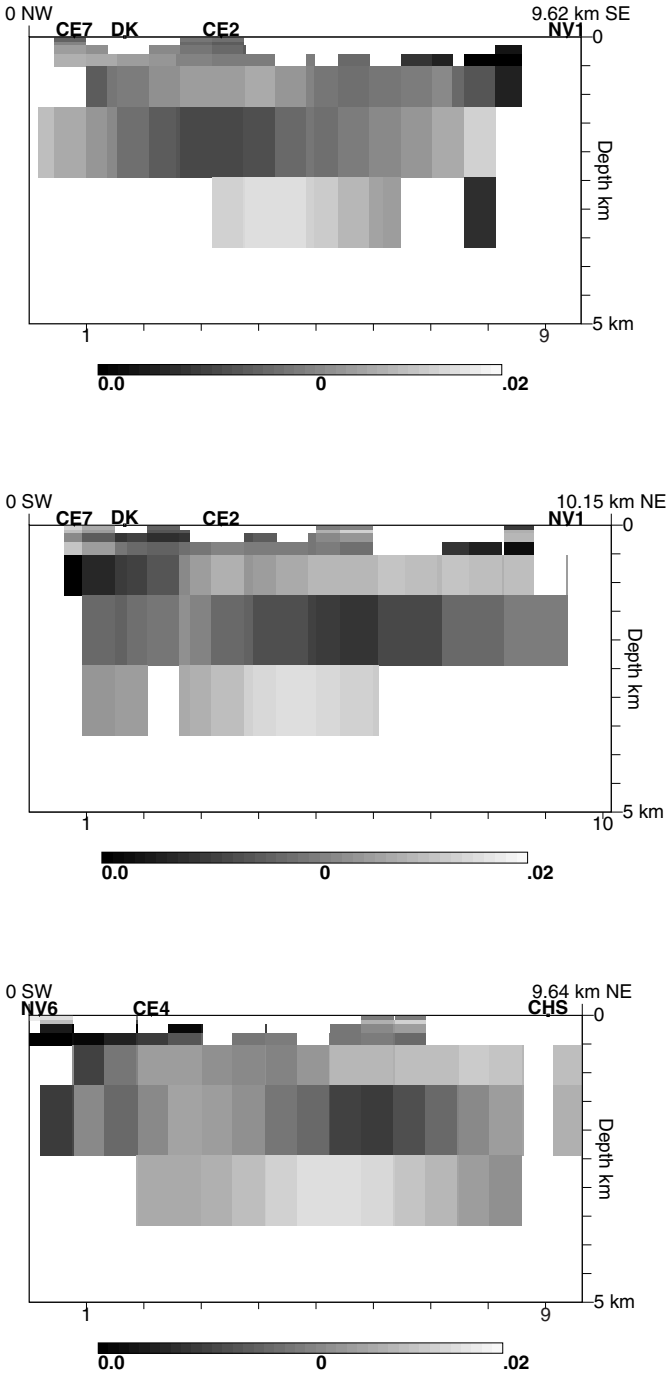

Figure 13. Vertical cross sections of Q anomalies in the Coso geothermal field. Locations of cross sections are presented in Figure 4, lower right.

scribed here. Because of the shallow seismicity, this data set, as yet, sheds little light on the shape and extent of the underlying magma body, or the deeper heat and magma sources for the Coso geothermal field. The imaging methodologies described here, however, can readily be applied to the more regional data set; for example, expanding the network and considering regional waveform phases may help in delineating the magma source. In the meantime, detailed lithologic, permeability, porosity, acoustic, and other geophysical borehole logs will allow testing of assertions and interpretations made regarding the seismic inversions outlined here. These will furthermore allow better characterization of future inversions and better monitoring of temporal variations of geophysical properties as the geothermal field evolves.

ACKNOWLEDGMENTS

I thank the Navy Geothermal Program for funding this project (award #N68936-94-R-0139) and providing data. I further acknowledge California Energy Co. Inc. and Peter Malin (Duke University) for data and valuable comments.

REFERENCES CITED

Alvarez, M.G., 1992, The seismotectonics of the southern Coso Range observed with a new borehole seismograph network [M.S. thesis]: Duke University.

Anderson, D.L., 1989, Theory of the earth: Boston, Blackwell Scientific, 366 p.

Babuska, V., and Cara, M., 1991, Seismic Anisotropy in the Earth, Modern Approaches in Geophysics: Dordrecht, Kluwer Academic, 217 p.

Bhattacharyya, J., Grosse, S., Lees, J.M., and Hasting, M., 1999, Recent earthquake sequences at Coso: Evidence for conjugate faulting and stress loading near a geothermal field: Bulletin of the Seismological Society of America, v. 89, p. 785–795.

Combs, J., 1980, Heat flow in the Coso geothermal area, Inyo County, California: Journal of Geophysical Research, v. 85, p. 2411–2424.

Crampin, S., 1984, Effective elastic constants for wave propagation through cracked solids: Geophysical Journal of the Royal Astronomical Society, v. 76, p. 135–145.

Feng, Q., and Lees, J.M., 1998, Microseismicity, stress, and fracture within the Coso geothermal field, California: Tectonophysics, v. 289, p. 221–238.

Gibson, R.L., Jr., and Toksoz, M.N., 1990, Permeability estimation from velocity anisotropy in fractured rock: Journal of Geophysical Research, v. 95, p. 15643–15655.

Hauksson, E., Hutton, K., Kanamori, H., Jones, L., Mori, J., Hough, S., and Roquemore, G., 1995, Preliminary report on the 1995 Ridgecrest earthquake sequence in eastern California: Seismological Research Letters, v. 66, p. 54–60.

Ho-Liu, P., Kanamori, H., and Clayton, R.W., 1988, Applications of attenuation tomography to Imperial Valley and Coso–Indian Wells region, southern California: Journal of Geophysical Research, v. 93, p. 10501–10520.

Hough, S.E., 1997, Empirical Green's function analysis: taking the next step: Journal of Geophysical Research, v. 102, p. 5369–5384.

Hough, S.E., Lees, J.M., and Monastero, F., 1999, Attenuation and source properties at the Coso geothermal area, California: Bulletin of the Seismological Society of America, v. 89, p. 1606–1619.

Hudson, J.A., 1981, Wave speeds and attenuation of elastic waves in material containing cracks: Geophysical Journal of the Royal Astronomical Society, v. 64, p. 133–150.

Hudson, J.A., 1994, Overall properties of anisotropic materials containing cracks: Geophysical Journal International, v. 116, p. 279–282.

Jackson, D.B., and ODonnell, J.E., 1980, Reconnaissance electrical surveys in the Coso Range, California: Journal of Geophysical Research, v. 85, p. 2502–2516.

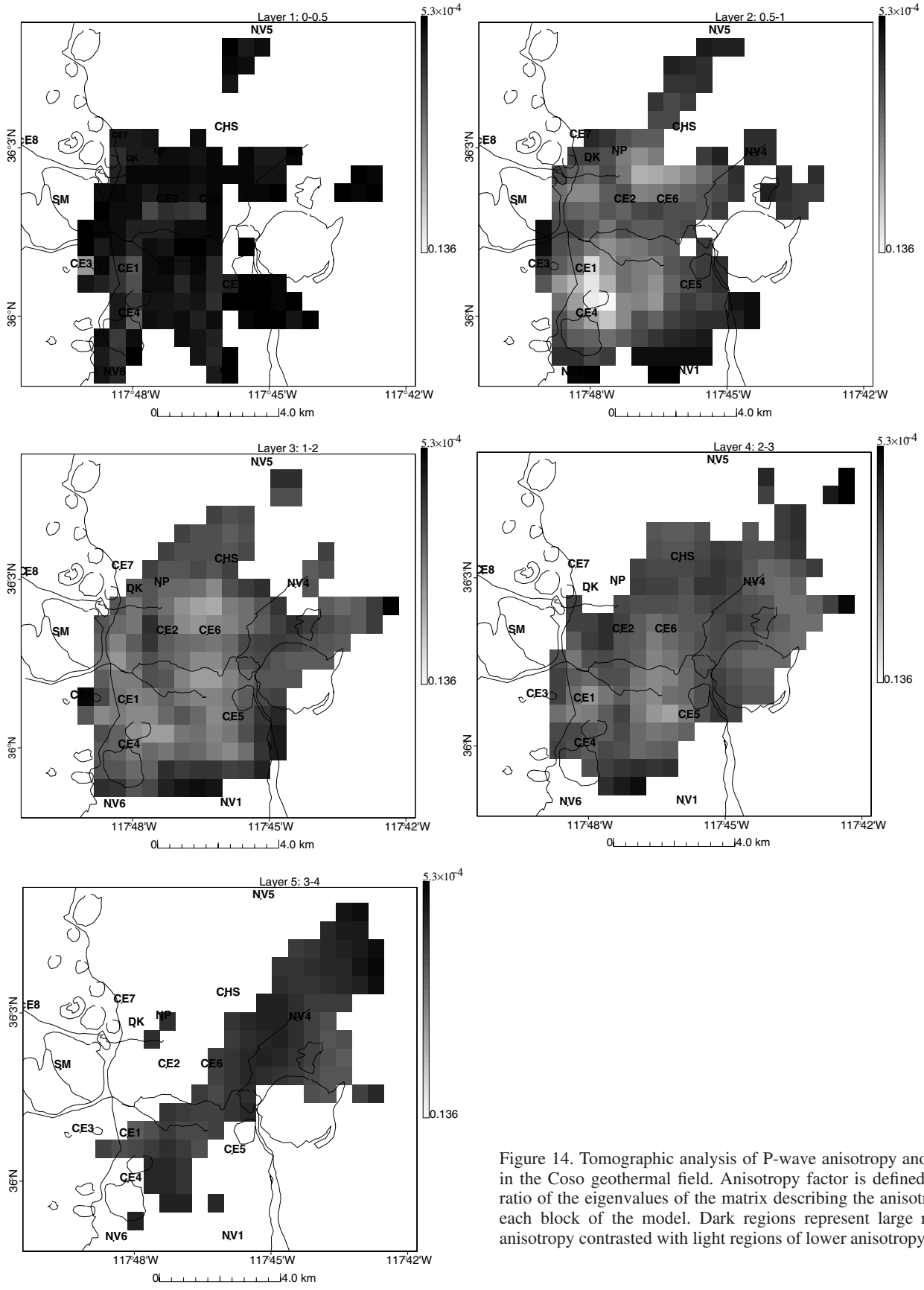

Figure 14. Tomographic analysis of P-wave anisotropy anomalies in the Coso geothermal field. Anisotropy factor is defined as the ratio of the eigenvalues of the matrix describing the anisotropy in each block of the model. Dark regions represent large relative anisotropy contrasted with light regions of lower anisotropy factor.

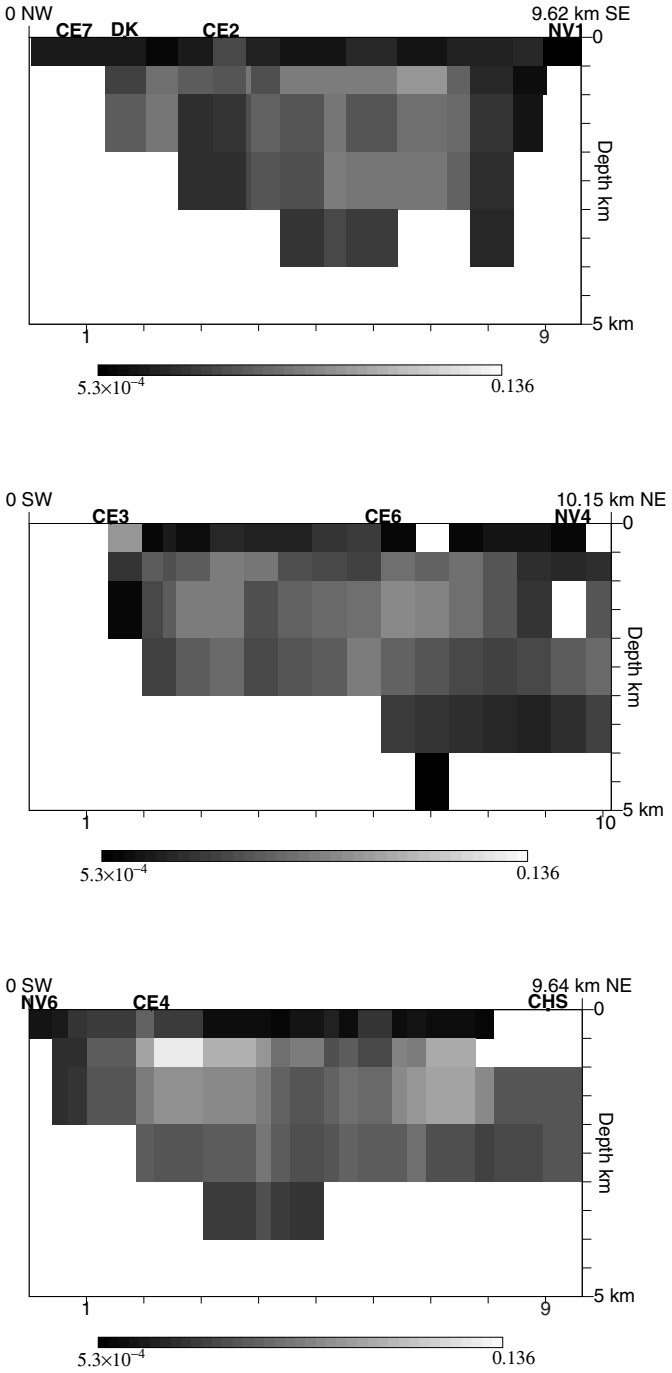

Figure 15. Vertical cross sections of P-wave anisotropy anomalies in the Coso geothermal field. Locations of cross sections are presented in Figure 4, lower right.

Johnston, D.H., Toksoz, M.N., and Timur, A., 1979, Attenuation of seismic waves in dry and saturated rocks: 2. Mechanisms: Geophysics, v. 44, p. 691–711.

Leary, P.C., and Henyey, T.L., 1985, Anisotropy and fracture zones about a geothermal well from P-wave velocity profiles: Geophysics, v. 50, p. 25–36.

Lees, J.M., 1992, The magma system of Mount St. Helens: Non-linear high resolution P-wave tomography: Journal of Volcanology and Geothermal Research, v. 53, p. 103–116.

Lees, J.M., 1997, Scattering from a vertical geothermal barrier at Coso, California: Seismological Research Letters, p. 318.

Lees, J.M., 1998, Multiplet analysis at Coso Geothermal: Bulletin of the Seismological Society of America, v. 88, p. 1127–1143.

Lees, J.M., and Crosson, R.S., 1989, Tomographic inversion for three-dimensional velocity structure at Mount St. Helens using earthquake data: Journal of Geophysical Research, v. 94, p. 5716–5728.

Lees, J.M., and Lindley, G.T., 1994, Three-dimensional attenuation tomography at Loma Prieta: Inverting t* for Q: Journal of Geophysical Research, v. 99, p. 6843–6863.

Lees, J.M., and Shalev, E., 1992, On the stability of P-wave tomography at Loma Prieta: A comparison of parameterizations, linear and non-linear inversions: Bulletin of the Seismological Society of America, v. 82, p. 1821–1839.

Lees, J.M., and Wu, H., 1999, P-wave anisotropy, stress, and crack distribution at Coso Geothermal Field, California: Journal of Geophysical Research, v. 104, p. 17955–17973.

Lees, J.M., and Wu, H., 2000, Poisson's ratio and porosity at Coso Feothermal Area, California: Journal of Volcanology and Geothermal Research, v. 95, p. 157–173.

Leslie, B.W., 1991, Decay series disequilibria applied to the study of rock-water interaction in the Coso Geothermal Field, California [Ph.D. thesis]: Univ. Southern California, 324 p.

Lou, M., and Rial, J.A., 1997, Characterization of geothermal reservoir crack patterns using shear-wave splitting: Geophysics, v. 62, p. 487–494.

Nur, A., 1971, Effects of stress on velocity anisotropy in rocks with cracks: Journal of Geophysical Research, v. 76, p. 2022–2034.

Nur, A., and Simmons, G., 1969, The effect of saturation on velocity in low porosity rocks: Earth and Planetary Science Letters, v. 7, p. 183–193.

Nur, A., Ron, H., and Beroza, G., 1993, Landers-Mojave earthquake line; a new fault system?: GSA Today, v. 3, p. 253, 256–258.

Pickett, G.R., 1963, Acoustic character logs and their applications in formation evaluation: Journal of Petroleum Technology, v. 15, p. 650–667.

Reasenberg, P., Ellsworth, W., and Walter, A., 1980, Teleseismic evidence for a low-velocity body under the Coso geothermal area: Journal of Geophysical Research, v. 85, p. 2471–2483.

Roquemore, G.R., and Simila, G.W., 1994, Aftershocks from the 28 June 1992 Landers earthquake; northern Mojave Desert to the Coso volcanic field, California: Bulletin of the Seismological Society of America, v. 84, p. 854–862.

Sanders, C., Ho, L.P., Rinn, D., and Kanamori, H., 1988, Anomalous shear wave attenuation in the shallow crust beneath the Coso volcanic region, California: Journal of Geophysical Research, v. 93, p. 3321–3338.

Schön, J.H., 1996, Physical properties of rocks: fundamentals and principles of petrophysics, *in* Helbig, K., and Treitel, S., eds., Handbook of geophysical exploration: Pergamon Press.

Tatham, R.H., 1982, Vp/Vs and lithology: Geophysics, v. 47, p. 333–344.

Walck, M.C., 1988, Three-dimensional variations in shear structure and Vp/Vs for the Coso region, California: Journal of Geophysical Research, v. 93, p. 2047–2052.

Walck, M.C., and Clayton, R.W., 1987, P wave velocity variations in the Coso region, California, derived from local earthquake travel times: Journal of Geophysical Research, v. 92, p. 393–405.

Walter, A.W., and Weaver, C.S., 1980, Seismicity of the Coso Range, California: Journal of Geophysical Research, v. 85, p. 2441–2458.

Wu, H., and Lees, J.M., 1992a, Application of the pseudo-spectral method for calculation of synthetic seismograms [abs.]: Eos (Transactions, American Geophysical Union), v. 73, p. 340.

Wu, H., and Lees, J.M., 1992b, Synthetic seismograms using finite elements for local earthquake data: A comparison with analytic and finite difference methods [abs.]: Eos (Transactions, American Geophysical Union), v. 73, p. 193.

Wu, H., and Lees, J.M., 1996, Attenuation structure of the Coso Geothermal area, California, from pulse width data of P-wave: Bulletin of the Seismological Society of America, v. 86, p. 1574–1590.

Wu, H., and Lees, J.M., 1997, Boundary conditions on a finite grid: Applications with pseudo-spectral wave propagation: Geophysics, v. 62, p. 1544–1555.

Wu, H., and Lees, J.M., 1999a, Cartesian Parameterization of Anisotropic traveltime tomography: Geophysical Journal International, v. 137, p. 64–80.

Wu, H., and Lees, J.M., 1999b, Three-dimensional *P* and *S* wave velocity structures of the Coso Geothermal Area, California, from microseismic traveltime data: Journal of Geophysical Research, v. 104, p. 13217–13233.

MANUSCRIPT ACCEPTED BY THE SOCIETY MAY 9, 2001

Printed in the U.S.A.